KSME Journal, Vol. 2, No. 1, pp. 35~43, 1988.

OBLIQUE SHOCK WAVES IN DUSTY GAS SUSPENSIONS

Y. Martsiano*, G. Ben-Dor* and O. Igra*

(Received February, 17, 1988)

The equations governing the flow field which is developed when a supersonic dusty-gas suspension passes through a straight oblique shock wave were formulated. A computer code for solving the governing equations was developed and used to obtain the solution for a variety of different initial conditions. In addition, the dependence of the post-shock suspension properties on the various physical properties of the dust particles, (namely the diameter of the dust particles, their specific heat capacity, their material density and the loading ratio of the dust in the suspension) was investigated.

Key Words : Gas Particle Suspension, Shock Wave, Gaseous Phase

NOMENCLATURE

A : Envelope area of the solid particle $=\pi D^2$
C : Specific heat capacity of the solid particle
C_D : Drag coefficient
C_P : Specific heat capacity at constant pressure of the gaseous phase
C_V : Specific heat capacity at constant volume of the gaseous phase
D : Diameter of the solid pariticle
F_D : Drag force
k : Thermal conductivity
M : Flow Mach number
m_p : Mass of a solid particle
N_u : Nusselt number
n : A co-ordinate normal to the oblique shock wave
n_p : Number density of the solid particles
P : Suspension pressure
P_r : Prandtl number
$Q_{H.T}$: Rate of heat per unit volume transferred from the gaseous to the solid phase
R : Specific gas constant
Re : Reynolds number
S : Cross section of the solid partcule $=nD^2/4$
T : Temperature
u : Velocity of gaseous phase
v : Velocity of the solid phase
y : Secific heat capaticies ratio $=C_p/C_v$
ϕ : Angle of incidence
β : Flow deflection angle
μ : Dynamic viscosity
ρ : Spatial density
σ : Material density
η : Loading ratio of the solid phase in the suspension $=\rho_{po}/\rho_{go}$

Subscripts

g : Gaseous phase
n : Normal component
p : Solid phase
s : Tangential component
x : Horizontal co-ordinate
y : Vertical co-ordinate
o : Flow state ahead of the shock wave
l : Flow state behind the shock wave

*The Pearlstone Center for Aeronautical Engineering Studies, Department of Mechanical Engineering,
Ben-Gurion University of Negev
Beer Sheva, 84105 P.O.Box. 653, Israel

1. INTRODUCTION

The interest in the gas-dynamic behaviour of a gas-particle suspension grew in the past three decades due to its application to many engineering problems. Some typical examples are: metallized propellents of rockets, jet-type dust collectors and blast waves in dusty atmospheres. In addition, mixtures with gases heavily laden with particles occur frequently in industrial processes such as plastics manufacturing, flour milling, coal-dust conveying, powder metallurgy and powdered-food processing. General descriptions of such flows can be found in several books and review papers [Soo (1967), Marble(1970) and Rudinger(1973)].

The major differences between the flow fields which are developed behind a normal shock wave in a dusty-gas and a pure (dust-free) gas are illustrated in Figs. 1a and b for the temperatures and the velocities, respectively. When a steady pure gas encounters a normal shock wave it experiences a sharp (almost discontinuous) change in its thermodynamic and kinematic properties. This sudden change is shown in Fig. 1 to occur between (0) and (1). The thickness of this disturbance, l_f, is only a few mean free paths of the gas atoms or molecules (about 6.6×10^{-6}cm in standard conditions). Beyond (1) the gas properties remain constant (solid lines in Figs. 1a and b) provided the gas conditions at (1) are not sufficient to excite the internal degrees of freedom of the gas.

If, however, the gas is laden with solid particles then the suspension which was originally at a state of thermodynamic and kinematic equilibrium, ahead of the shock front, is sud-

denly changed into a non-equilibrium state, because the solid particles, due to their size compared with l_f do not experience any noticeable change in their properties upon moving from (0) to (1). Thus, at (1) the gas has a much higher temperature than the dust, $T_g \gg T_p$ and a much lower velocity $u \ll v$. Morgenthaler (1962) indicated that this is true even if the particle diameter is as small as 0.1 μm (for shock waves in air at nearly standard conditions, where the mean free path is about 0.066μm). Therefore, the particles are not influenced by the initial disturbance, and the gas properties at (1) can be safely assumed to be indentical to those of a pure gas with the same initial conditions.

For downstream of (1), i.e., at (∞) in Fig. 1, the gas and the solid phases reach a new state of thermodynamic and kinematic equilibrium via momentum and energy exchange. Theoretically all shock waves in dusty gases are infinitely thick, since equilibrium is approached asymptotically. However, it is a common practice to assign to the shock wave an effective thickness which is defined by a requirement that the suspension propertices come close to their equilibrium downstream values. It was shown by Gottlieb and Coskunses (1985) that the suspension equilibrium properties (at infinity) can be calculated from the usual normal shock wave relations, provided that the usual pure gas parameters $\bar{\gamma}$ and $\bar{R}$ (the specific heat capacities ratio and the specific gas constant) are replaced by effective values γ and R which solely depend on the initial conditions of the suspension.

Between (1) and (∞) the solid particles are not in equilibrium with the gas. The flow region between (1) and ∞ is known as the relaxation zone, for it is analogous to the relaxation zone in pure gases where the internal degrees of freedom are excited. The extent of the relaxation zone strongly depends on the momentum and heat transfer mechanisms which enable the solid and the gaseous phases to reach a new equilibrium state. The analysis of the relaxation zone was studied by many investigators. The pioneering works of Carrier (1958), Kriebel (1964) and Rudinger (1964) verified the existence of this relaxation zone and identified the parameters affecting it, namely; the solid particle diameter, D, its specific heat capacity, C, its material density, σ, and the loading ratio, η. Igra and Ben-Dor (1980) compared various correlations for the drag coefficient, C_D, and the heat transfer coefficient, Nu, and pointed out their effect on the extent of the relaxation zone. In addition they studied the role of thermal radiation heat transfer between the two phases and showed that it can be neglected when the incident shock waves Mach number is smaller than five.

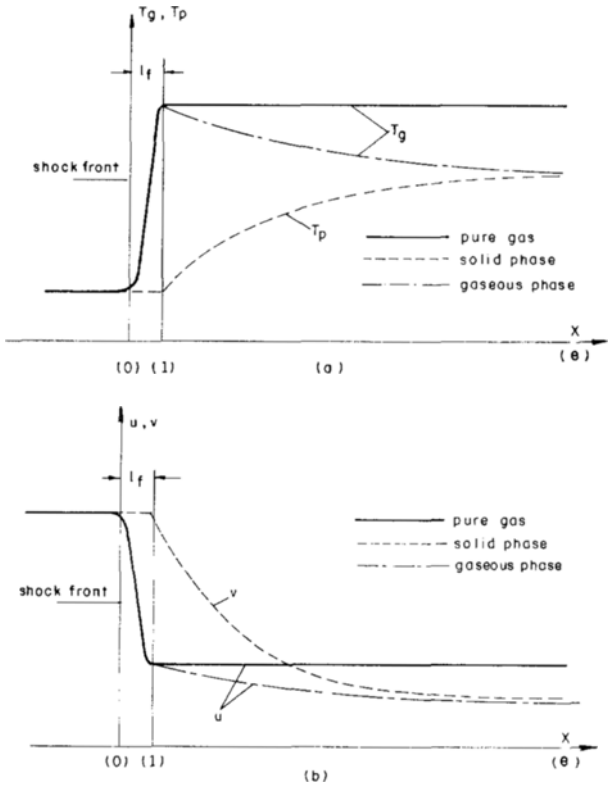

Fig. 1 The shock wave structure in a pure (solid lines) and a dusty (dashed line) gas. (a) Temperature profiles (b) Velocity profiles

In all the above mentioned works, as well as in many others, the gaseous phase was assumed to behave as a perfect gas. This assumption was relaxed by Ben-Dor and Igra(1982) and Igra and Ben-Dor(1984) who solved the flow field while accounting for real gas effects. Dissociating nitrogen was the gaseous phase in the latter work and ionizing argon in the former.

The assumption that the solid particles are inert, which was also adopted in most of the published studies, was relaxed by Elperin, Ben-Dor and Igra(1986) who solved the flow field of an oxygen-carbon suspension passing through a normal shock wave, behind which the temperature of the carbon particles reached their ignition temperature and burned out.

The assumption of uniform solid particles was relaxed by Elata, Ben-Dor and Igra(1988) who solved the case of size-distributed solid particles.

In all the above mentioned solutions the flow field was one-dimensional and steady. The aim of the present study was to solve the case of a two-dimensional steady flow. This is the case when the shock wave is oblique. There are many incidences where the shock wave is oblique. For example, one can mention the shock wave generated by a supersonic vehicle, the shock wave which is developed at the entrance nozzle of a rocket engine and the reflected shock waves which arise when an explosion generated blast wave interacts with man-made structures. in all these cases the shock wave is oblique and, hence, unlike the previously mentioned cases the resulted flow field behind the shock wave is two-dimensional.

The aim of the present study, therefore, is to solve the flow field which is developed when a supersonic dusty gas suspension passes through a straight oblique shock wave.

Figure 2 illustrates schematically the problem to be solved. A dust gas suspension which is in a thermal and kinematic equilibrium encounters an oblique shock wave. The angle of incidence is ϕ (sometimes known as the wave angle). As mentioned previously, upon the passage of the suspension through the shock wave, the properties of the gaseous phase assume a new state, known as the frozen state, immediately behind the shock front, while the solid phase passes through the shock wave unaffected. due to the fact that the shock wave is oblique, the streamline of the gaseous phase is deflected by an angle, θ_g, while the trajectory of dust particles of the two phases which were mentioned previously, here there is also a difference in the direction of propagation of the two phases. The two phases which are no longer in equilibrium, start exchanging momentum and energy until they

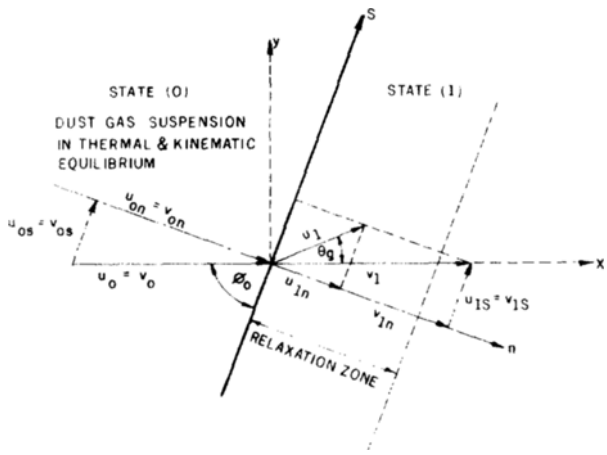

Fig. 2 A schematical illustration of an oblique shock wave in a dusty gas and the definition of the (x, y)-and (n, s) -planes.

finally reach a new thermal and kinematic equilibrium. Here, kinematic equilibrium means that, in addition to equal velocities, the two phases also reach the same direction. The flow region inside which the two phases are in non-equilibrium, i. e., the relaxation zone, is also shown in Fig. 2.

2. THEORETICAL BACKGROUND

2.1 Assumptions

The assumptions upon which the present model is based and their implications are listed in the following:

(1) The gaseous phase behaves as an ideal gas. Thus, the equation of state of the gas is $P=\rho_g RT_g$. Note that it is not assumed here that the gas is calorically ideal. Alternatively, the dependence of both C_p and C_v on the gas temperature is accounted for. This has not been done in previous studies where both C_p and C_v were assumed to be constant.

(2) All solid particles are rigid, inert small identical spheres uniformly distributed in the gaseous phases. Thus there is no heat addition or reduction due to chemical processes between the solid and the gaseous phases. Furthermore, Re and Nu are based on the particle diameter, D.

(3) The volume of the solid phase in the suspension can be neglected. Thus the momentum and energy exchange among the solid particles can be ignored.

(4) Aside from momentum and energy interactions between the gaseous and the solid phases, the gaseous phase is considered to be a perfect flow, i.e., the dynamic viscosity, μ_g, and the thermal conductivity, k_g, are zero. This also implies that neither kinematic nor thermal boundary layers develop around the solid particles.

(5) The dynamic viscosity, μ_g, the thermal conductivity, k_g, and the specific heat capacity at constant pressure, C_p, of the gaseous phase depend solely on its temperature, T_g.

(6) The solid particles are too large to experience any change in their thermodynamic and dynamic properties upon their passage through the shock front. In addition they are also large enough not to experience Brownian motion. Thus, the partial pressure of the solid phases can be neglected.

(7) The solid particles are small enough to satisfy the condition $B_i<0.1$, where B_i is the Biot number, $B_i=hr/k_p$ (h is the coefficient of connection heat transfer, r is the radius of the solid particle, and k_p is its thermal conductivity). Thus the temperature within the solid particles can be assumed to be uniform.

(8) The weight of the solid particles and the buoyancy forces experienced by them are negligibly small in comparison with the drag forces acting on them.

(9) The specific heat capacity, C, of the solid particles is constant.

(10) Ahead of the normal shock wave the suspension is at a state of thermodynamic and kinematic equilibrium, i.e., $u_o=v_o$ and $T_{go}=T_{po}$, where u and v are the velocities of the gas and the solid particles, and T_g and T_p are the temperatures of the gaseous and solid phases, respectively.

(11) Based on the density ratio of the two phases 1/2500, the virtual mass which depends on this ratio is neglected.

In addition to the above listed assumptions it is assumed that the flow field under consideration is two-dimensional and steady.

If the entire problem is analyzed in the (s, n)-plane, where the s-axis is parallel to the shock wave front and the n-axis is normal to the shock wave front, then the problem at hand can be considered as one-dimensional. Note that the s-component of the velocities of the two phases immediately behind the shock front are identical, i.e., $u_{1s}=v_{1s}$. For this reason the relative velocity between the two phases in the s-direction. is zero, and therefore there are no drag forces in the s-direction. As a consequence, there are no changes in the velocity components in the s-direction and they remain constant in the entire flow field. From symmetrical considerations, it is obvious that all the properties of the suspension must remain constant along $n=$constant lines, i.e., along lines which are parallel to the s-axis. Therefore, the partial derivative of any of the suspension properties with respect to s is zero.

2.2 Governing Equations

Based on the foregoing discussion and assumptions, the governing equations for the problem at hand are:

-conservation of mass of the gaseous phase:

$$\frac{d}{dn}(\rho_g u_n)=0 \tag{1}$$

-conservation of mass of the solid phase:

$$\frac{d}{dn}(\rho_p v_n)=0 \tag{2}$$

-conservation of linear momentum of the gaseous phase:

$$\rho_g v_n \frac{du_n}{dn}+\frac{dP}{dn}=F_{Dn} \tag{3}$$

-conservaton of linear momentum of the solid phase:

$$\rho_p v_n=\frac{dv_n}{dn}=-F_{Dn} \tag{4}$$

-conservation of energy of the gaseous phase:

$$\rho_g u_n \frac{d}{dn}(C_p T_g+\frac{1}{2}u_n^2)=Q_{H.T}+F_{Dn}v_n \tag{5}$$

-conservation of energy of the solid phase:

$$\rho_p v_n \frac{d}{dn}\left(CT_p+\frac{1}{2}v_n^2\right)=-Q_{H.T.}-F_{Dn}v_n \tag{6}$$

where ρ_g and ρ_p are the spatial densities of the gaseous and solid phases, u_n and v_n are the velocity components of the gaseous and solid phases in the n-direction, T_g and T_p are the temperatures of the gaseous and solid phases, P is the pressure of the suspension, C_p is the specific heat capacity at constant pressure of the gaseous phase, C is the specific heat capacity of the soild particles, $Q_{H.T}$ is the amount of heat transferred per unit volume from the gaseous phase to the solid phase and F_{Dn} is the drag force per unit volume applied by the gaseous phase on the solid particles.

Thus, if C_p, C, $Q_{H.T}$ and F_{Dn} are expressed in terms of the dependent variables namely; ρ_g, ρ_p, u_n, v_n, T_g, T_p and P, then the above set of six conservation equations contain seven unknowns. The seventh equation which is required to make the above set of equations solvable, is the equation of state of the gaseous phase; i.e.,

$$P=\rho_g R T_g \tag{7}$$

In the following, the above mentioned complementary equations are developed.

The drag force per unit volume can be obtained by multiplying the drag force acting on a single solid particle by the number density of the solid particles.

$$F_{Dn}=\frac{1}{2}\rho_g C_D(v_n-u_n)\cdot|v_n-u_n|\cdot S n_p \tag{8}$$

where C_D is the drag coefficient, S is the projected cross section of the solid spherical particle (i.e., $S=\pi D^2/4$, where D is the diameter of the solid particles), and n_p the number density of the solid particles can be calculated from

$$n_p=\frac{\rho_p}{m_p} \tag{9}$$

where m_p is the mass of a single solid particle (i,e., $m_p=\sigma\pi D^3/6$, where σ is the material density of the solid particles).

The drag coefficient, C_D, is usually expressed as a function of the Reynolds number, Re, which in turn depends on the slip velocity $|v_n-u_n|$. For this reason, the Re number is very high immediately behind the shock wave while its magnitude vanishes towards the end of the relaxtion zone, where $v_n\approx u_n$, is approached. For this reason two different correlations for the drag coefficient C_D are used:

For $Re<800$

$$C_D=\frac{24}{Re}(1+0.15Re^{0.687}) \tag{10a}$$

and for $800<Re<3\times10^5$

$$C_D=\frac{24}{Re}(1+0.15Re^{0.687})+\frac{0.42}{1+42500\ Re^{-1.16}} \tag{10b}$$

Both of these correlations were taken from Clift, Grace and Weber (1978). The Reynolds number is calculated from:

$$Re=\frac{\rho_g|v_n-u_n|D}{\mu_g} \tag{11}$$

where μ_g, the dynamic viscosity of the gaseous phase, is calculated by the expression suggested by Mazor, Ben-Dor and Igra(1985) which reads:

$$\mu_g=\mu_{gr}\left(\frac{T_g}{T_{gr}}\right)^{0.65} \tag{12}$$

where μ_{gr} is the dynamic viscosity of the gaseous phase at a reference temperature T_{gr}.

The heat transferred per unit volume from the gaseous phase to the solid phase can be obtained by multiplying the heat transferred to a single particle by the number density of the solid particles, i.e.,

$$Q_{H.T.}=Ah(T_p-T_g)n_p \tag{13}$$

where A is the surface area of the solid spherical particle (i.e., $A=\pi D^2$) and h the coefficient of heat convection can be calculated from

$$h=\frac{Nuk_g}{D} \tag{14}$$

where k_g is the thermal conductivity of the gaseous phase and Nu the Nusselt number is a function of the Reynolds number, Re, and the Prandtl number, Pr, which is defined as

$$Pr=\frac{\mu_g C_p}{k_g} \tag{15}$$

The correlation for Nu which was used in the present study is taken from Drake (1961). It reads:

$$Nu=2+0.459Pr^{1/3}Re^{0.55}$$

As mentioned in assumption (5) the specific heat capacity at constant pressure, C_p, and the thermal conductivity, k_g, depend solely on the temperature of the gaseous phase, T_g. For this reason the gaseous phase was identified as air. For (Holman, 1981, p. 542) in the range $300<T_g<2500K$

$$k_g=0.0125+5.509\times10^{-5}T_g \tag{16}$$

and from Van Wylen and Sonntag (1978) p. 683

$$C_p=39.06-512.79\left(\frac{T_g}{100}\right)^{-1.5}+1072.7\left(\frac{T_g}{100}\right)^{-2}-820.4\left(\frac{T_g}{100}\right)^{-3}$$

this condition is good for $300<T_g<3500K$.

2.3 Numerical Solution

Now we are at the stage where the governing equations are well defined, i.e., the number of independent variables is equal to the number of equations and all the non-dependent variables can be expressed in terms of the dependent variables and other known parameters.

As can be seen, the governing equations of the problem at hand consist of seven non-linear differential equations which must be solved simultaneously in order to obtain the spatial distribution of the flow properties.

Numerous computer code packages, capable of numerically solving non-linear differential equations, are available,

e.g., the IMSL (International Mathematical and Statistical Libraries). This package contains three different computer codes for solving a given set of differential equations provided the initial conditions are known. (As will be shown subsequently, the initial conditions in the case at hand are indeed known.) The most accurate code out of these three codes is DREBS. It is based on the extrapolation method, and is superior when very high accuracy is required and when the calculation of the derivatives is not expensive.

Fortunately, the relative simplicity of the governing equations of the problem at hand, enables one to rewrite them in a form where the derivatives of the dependent variables are isolated, and hence can be calculated very quickly and cheaply (computer-wise). The rewritten set of the governing equations can be changed to the following form:

$$\frac{dT_g}{dn}=\frac{Q_{H.T.}+F_{Dv}-\dfrac{F_D\,u^3}{u^2-RT_g}}{\rho_g u\left[C_p-\dfrac{R\,u^2}{u^2-RT_g}\right]} \tag{17}$$

$$\frac{du}{dn}=\frac{F_D-\rho_g R\dfrac{dT_g}{dn}}{\rho_g\dfrac{u-RT_g}{u}} \tag{18}$$

$$\frac{dP}{dn}=\rho_g R\left(\frac{dT_g}{dn}-\frac{T_g}{u}\frac{du}{dn}\right) \tag{19}$$

$$\frac{d\rho_g}{dn}=-\frac{\rho_g}{u}\frac{du}{dn} \tag{20}$$

$$\frac{dT_p}{dn}=-\frac{Q_{H.T.}}{c\rho_p v} \tag{21}$$

$$\frac{dv}{dn}=-\frac{F_D}{\rho_p v} \tag{22}$$

$$\frac{d\rho_p}{dn}=-\frac{\rho_p}{v}\frac{dv}{dn} \tag{23}$$

2.4 The Initial Conditions

As mentioned earlier, the problem at hand is such that the initial conditions, i.e., the values of the dependent variables at $x=0$[at state (1) in Fig. 1] can be easily calculated.

Based on the fact that the thickness of the shock wave front is orders of magnitude smaller than the diameter of the solid particles, it is a common practice to assume that:

(1) The gaseous phase experiences the well known "frozen" change upon its passage through the shock wave.

(2) The solid phase remains unaffected as it passes through the shock wave. The above assumptions imply that while the properties of the solid phase immediately behind the shock wave front are identical to those ahead of it, the properties of the gaseous phase can be calculated using the well known Rankine-Hugoniot relations which relate the gas properties in both sides of the shock wave. More specifically;

$$\rho_{g1}=\rho_{g0}\left[\frac{(\gamma+1)M_0^2}{(\gamma-1)M_0^2+2}\right] \tag{24}$$

$$P_1=P_0\left[\frac{1}{\gamma+1}(2\gamma M_0^2-\gamma+1)\right] \tag{25}$$

$$T_{g1}=T_{g0}\left[\frac{\left(1+\dfrac{\gamma-1}{2}M_0^2\right)\left(\dfrac{2\gamma}{\gamma-1}M_0^2-1\right)}{\dfrac{(\gamma+1)^2}{2(\gamma-1)}M_0^2}\right] \tag{26}$$

$$M_1=\frac{M_0^2+\dfrac{2}{\gamma-1}}{\dfrac{2\gamma}{\gamma-1}M_0^2-1} \tag{27}$$

$$u_1=M_1\sqrt{\gamma RT_{g1}} \tag{28}$$

where subscripts "0"and "1" denote the flow states immediately ahead and behind the shock wave. M is the Mach number of the gaseous phase, i.e., $M=u/a$ [a, the local speed of sound, is simply calculated from $a=(\gamma RT)^{1/2}$].

Note that when $M_0\to 1$, i.e., when the shock wave degenerates to a Mach wave, then there is no change in the properties of the gaseous phase as it passes through the shock wave.

Since the model at hand assumes that the gaseous phase behaves as a perfect gas the upper value of M_0 which can be used is limited, since as $M_0\to\infty$ $T_g\to\infty$. In the case of a diatomic gas, such as oxygen (O_2), nitrogen (N_2), etc, $M_0=6$ is usually taken as the upper limit for which the assumption of a perfect gas behaviour is valid. For monatomic gases such as helium (He), neon (Ne), argon (Ar), etc., the upper limit or M_0 is even higher. Beyond these limiting values, real gas effects must be accounted for. The ways of treating such cases are discussed by Ben-Dor and Igra (1982) and Igra and Ben-Dor (1984).

2.5 Complementary Equations

Once the set of the governing equations is solved, the velocity vectors of each of the two phases can be calculated from:

$$\vec{u}=u_n\hat{n}+u_s\hat{s} \tag{29a}$$

$$\vec{v}=v_n\hat{n}+v_s\hat{s} \tag{29b}$$

The absolute velocities of the two phases are therefore:

$$|\vec{u}|=(u_n^2+u_s^2)^{1/2} \tag{30a}$$

$$|\vec{v}|=(v_n^2+v_s^2)^{1/2} \tag{30b}$$

The deflection of the gaseous phase streamline, θ_g, from its original direction can be calculated from

$$\theta_g=\phi-\tan^{-1}\frac{u_n}{u_s} \tag{31a}$$

Similarly, the deflection of the dusty phase streamline, θ_p, is

$$\theta_p = \phi - \tan^{-1}\frac{v_n}{v_s} \tag{31b}$$

Obviously, when the suspension reaches a new equilibrium state at the end of the relaxation zone the flow directions of the two phases become parallel and hence $\theta_{g\infty} = \theta_{p\infty}$

The velocity components of the gaseous and the dusty phases in the (x, y)-coordinate system shown in Fig. 1 can be calculated from:

$$u_x = u_n \sin\phi + u_s \cos\phi \tag{32a}$$

$$u_y = -u_n \cos\phi + u_s \sin\phi \tag{32b}$$

and similarly for the solid phase:

$$v_x = v_n \sin\phi + v_s \cos\phi \tag{33a}$$
$$v_y = -v_n \cos\phi + v_s \sin\phi \tag{33b}$$

2.6 Numerical Results

As mentioned earlier, the problem at hand can be treated as one-dimensional by solving it in the (s, n)-plane. For this reason, the flow profiles shown in Igra and Ben-Dor (1980), for example, are all applicable for the case of oblique shock waves, provided the flow Mach number M_0 is replaced by $M_0 \sin\phi$ and the x-axis is replaced by the n-axis. Note that if the angle of incidence is set to $\phi = 90^0$, then the oblique shock wave becomes normal to the oncoming flow, and the general case of an oblique shock wave degenerates to the well known one-dimensional normal shock wave case.

Since the change of the flow properties in a direction normal to the oblique shock wave front as well as the dependence of these properties on the physical properties of the dust particles can be deduced from Igra and Ben-Dor (1980), in the following only results which are unique to the fact that the shock wave is oblique are presented.

2.7 The Gas Deflection-θ_g

As mentioned earlier, the direction of the streamline of the gaseous phase changes continuously from its "frozen" direction to its "equilibrium" direction. In the following, the dependence of the flow deflection angle, θ_g, on the physical properties of the dust is discussed.

The dependence of the flow deflection, θ_g, on the dust loading ratio, η, is illustrated in Fig. 3, for $M_0 = 3$ and $\phi = 30^0$. The dust physical parameters are $D = 100\mu$m, $C = 1000 J/$(Kgmk), $\sigma = 1500$Kgm/m^3.

As can be seen the frozen value of θ_g, i.e., θ_g at $n = 0$ is identical for all the cases. However, the larger the loading ratio is, the greater the equilibrium flow deflection becomes. The dashed lines are the values calculated by the equivalent gas concept presented in the introduction, which should be reached at the end of the relaxation zone.

It is also evident from Fig. 3 that the larger the loading ratio is, the shorter the relaxation length becomes. While for $\eta = 0.1$ it takes about 8m for the gaseous phase to reach the equilibrium deflection angle, only 3m are required when $\eta = 2$.

The deflection angle at the end of the relaxation zone, $\theta_{g_{eq}}$, as a function of the dust loading ratio, η, is shown in a different way in Fig. 4 for $M_0 = 4$, $\phi = 60^0$, $D = 100\mu$m, $C = 1000$J/(KgmK) and $\sigma = 1500$Kgm/m^3.

The fact that the equilibrium deflection angle increases with increasing loading ratios is clearly seen in Fig. 4.

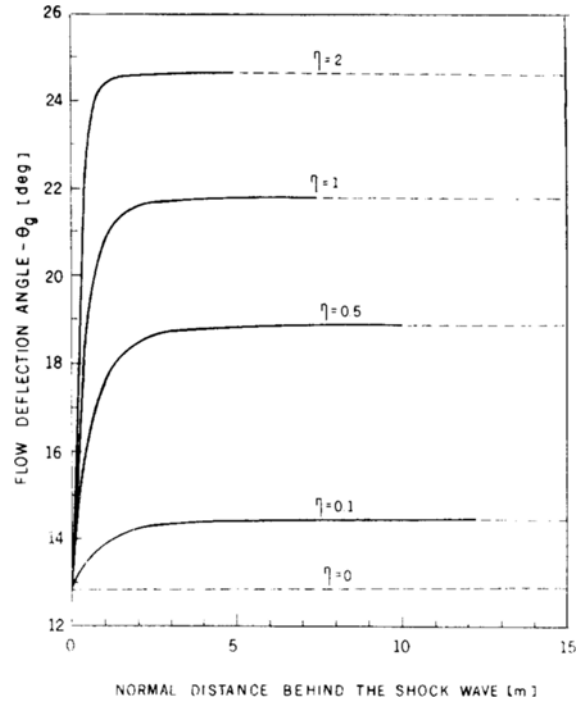

Fig. 3 The change of the flow deflection angle θ_g with normal distance from the shock wave for various loading ratios η and $M_0 = 3$, $\phi = 30^0$, $D = 100\mu$m, and $C = 1000$J/(Kgm K).

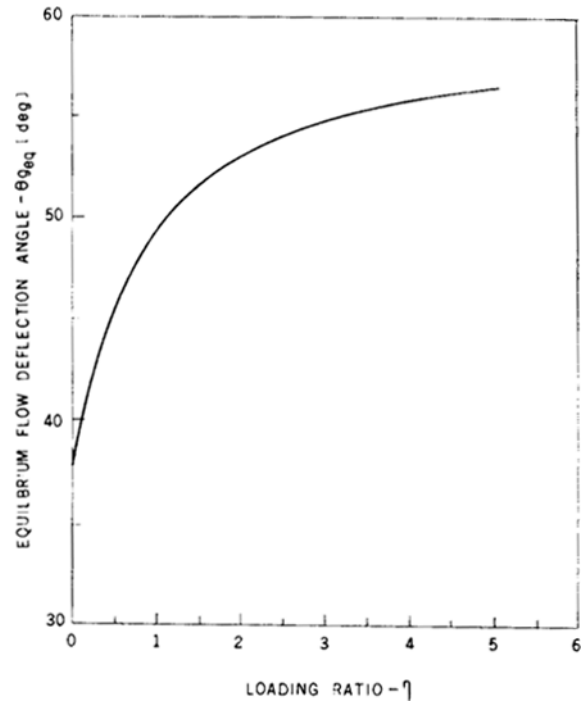

Fig. 4 The equilibrium flow deflection angle, $\theta_{g_{eq}}$, as a function of the loading ratio, η, for $M_0 = 4$, $\phi = 60^0$, $D = 100\mu$m, and $C = 1000$J/(Kgm K).

However, it is evident that as η increases the rate of increase of the equilibrium deflection angle decreases and it seems that there is an upper limit on $\theta_{g_{eq}}$ as η assumes very high values.

The dependence of the deflection angle, θ_g, on the diameter

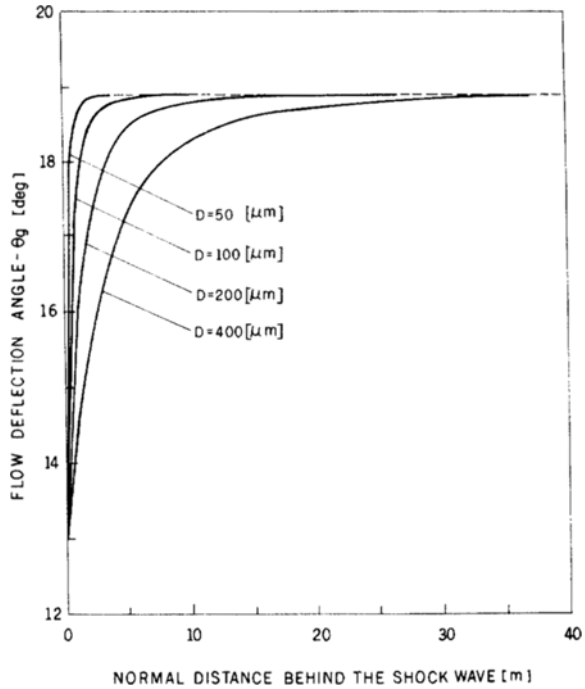

Fig. 5 The change of the flow deflection angle with normal distance from the shock wave for various solid particle diameters, D, $M_0=3$, $C=1000$J/(Kgm K), $\phi_0=30^\circ$, and $\eta=0.5$.

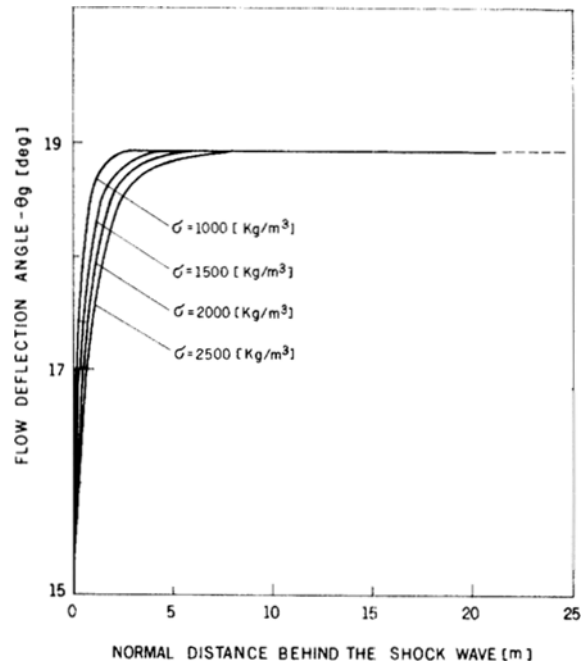

Fig. 7 The change of the flow deflection angle with distance from the shock wave for various values of material density of the solid particles, σ, and $M_0=3$, $\phi_0=30^\circ$, $D=100\mu$m, $C=1000$J/(Kgm K), and $\eta=0.5$.

of the solid particles is shown in Fig. 5. Again $M_0=3$ and $\phi=30^\circ$. The dust properties are $\eta=0.5$, $C=1000$J/(Kgm K) and $\sigma=1500$Kgm/m^3.

Since the loading ratio, η, and the specific heat capacity of the dust particles, C, are the same for the cases, the equilibrium values at the end of the relaxation zone are identical. However, it is evident from Fig. 5 that the smaller the diameter of the solid particle is, the shorter the relaxation length becomes.

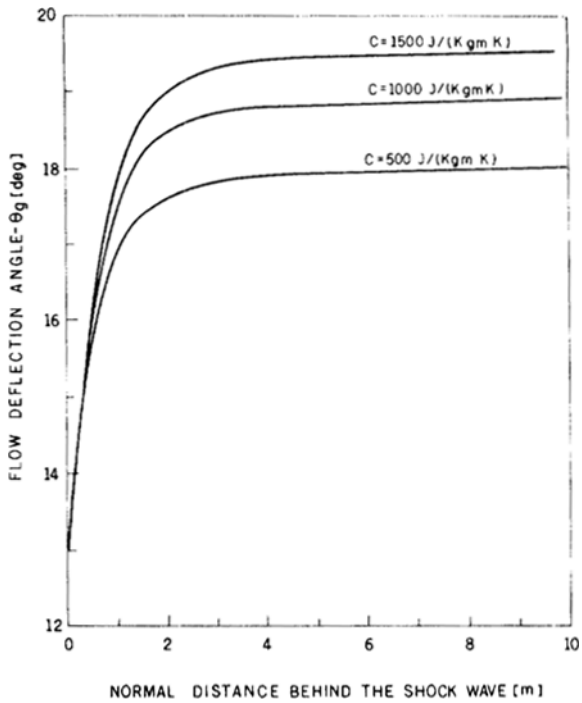

Fig. 6 The change of the flow deflection angle with normal distance from the shock wave for various values of specific heat capacity of the solid particles, C, and $M_0=3$, $\phi_0=30^\circ$, $D=100\mu$m, and $\eta=0.5$.

The dependence of the deflection angle, θ_g, on the specific heat capacity of the solid particles, C, for $M_0=3$ and $\phi=30^\circ$ is shown in Fig 6. The properties of the solid phase are $\eta=0.5$ $D=100\mu$m and $\sigma=1500$Kgm/m^3. It is evident from Fig. 6 that higher values of the specific heat capacities result in larger deflections at the end of the relaxation zone. The length of the relaxation zone is not seen to strongly depend on the specific heat capacity.

The dependence of the deflection angle, θ_g, on the material density of the soild particles for $M_0=3$ and $\phi=30^\circ$ is shown in Fig. 7. The dust properties are $\eta=0.5$, $D=100\mu$m, $C=1000$J/(Kgm K). Again, since η and C are identical for all the cases, the equilibrium values approached towards the end of the relaxation zone are the same for all the calculated cases. It is clearly seen from Fig. 7 that the smaller the material density is, the shorter the relaxation zone becomes. While it is about 4m for $\sigma=1000$Kgm/m^3 it increases to about 10m when σ is increased to 2500Kgm/m^3.

The gas and the solid particle paths is shown in Fig. 8 for $M_0=3$, $\phi=60^\circ$, $\eta=1.0$, $D=100\mu$m, $C=1000$J/(Kgm K) and $\sigma=1500$Kgm/m^3. The difference between the trajectories is clearly evident. While the gas particles are deflected immediately upon their passage through the shock wave ($n=0$), the solid particles do not change their original direction. However, behind the shock front the streamlines of the two phases approach a parallel direction. The results shown in Fig. 8 indicate that it is impossible to shape a wedge in a supersonic flow of a dusty gas, in such a way that it will generate a straight oblique shock wave. This is due to the fact that a

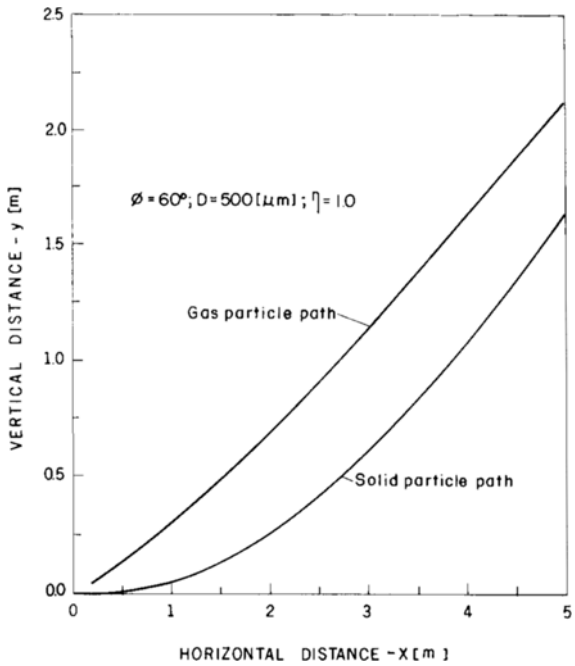

Fig. 8 The gas and solid particles paths in the (x, y)-plane for $M_0=3$, $\phi_0=60^0$, $D=500\mu$m, $C=1000$J/(Kgm K), $\sigma=1000$Kgm/m^3, and $\eta=1$.

straight oblique shock wave in a dusty gas results in two different particle trajectories, and no wedge can satisfy these two profiles. However, if the wedge surface is sticky, i.e., if it can be assumed that when a solid particle hits the surface, it sticks to it, then a wedge having a profile identical to that of the gas particle path might generate a straight oblique shock wave. It should be noted, however, that in the case of a sticky wedge surface, solid particles are drawn away from the suspension and hence their loading ratio η could be affected.

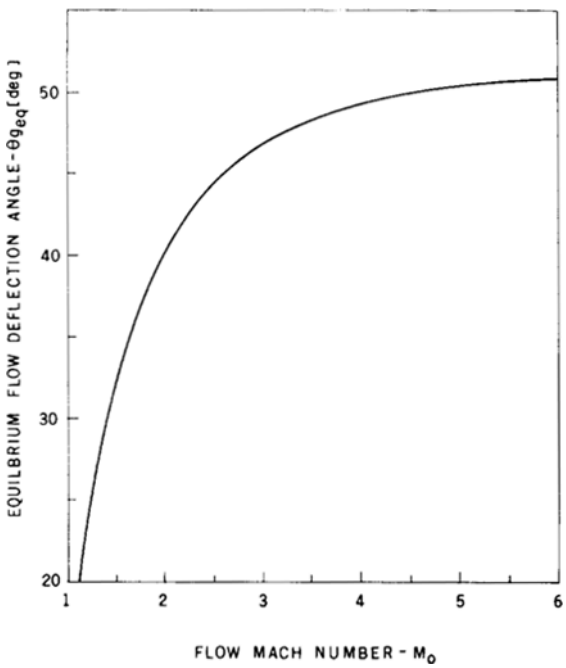

Fig. 9 The dependence of the equilibrium flow deflection angle, $\theta_{g_{eq}}$, on the incident flow Mach number, for $\phi=60^0$, $D=200\mu$m, $C=1000$J/(Kgm K), $\sigma=1000$Kgm/m^3 and $\eta=1$.

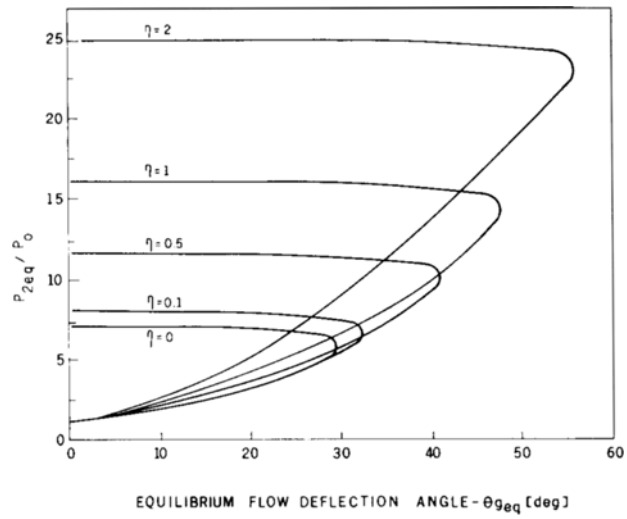

Fig. 10 The (P, θ_g)-shock polar for $M_0=2.5$, $D=100\mu$m, $C=1000$J/(Kgm K), $\sigma=1000$Kgm/m^3, and different values of the loading ratio η.

The dependence of the equilibrium deflection angle, $\theta_{g_{eq}}$, on the flow Mach number, M_0, is shown in Fig 9 for $\phi=60^0$, $\eta=1$, $D=200\mu$m, $C=1000$J/(Kgm K) and $\sigma=1500$Kgm/m^3. It is evident from this figure that the equilibrium deflection angle increases as the flow Mach number increases. However, as the flow Mach number reaches high values, the equilibrium deflection angle is seen to approach an upper limit.

It is a common practice to use shock polars to study oblique shock waves. Thus, in the following, shock polars in dusty gas suspension are presented.

The (P, θ_g)-polar for the case $M_0=2.5$, $D=100\mu$m, $C=1000$J/(Kgm K), $\sigma=1500$Kgm/m^3 and various values of η are shown in Fig 10. The (P, θ_g)-polar in this case represents the conditions at the end of the relaxation zone, i.e., $P=P_{eq}$ and $\theta_g=\theta_{g_{eq}}$. As can be seen the equilibrium pressure, P_{eq},

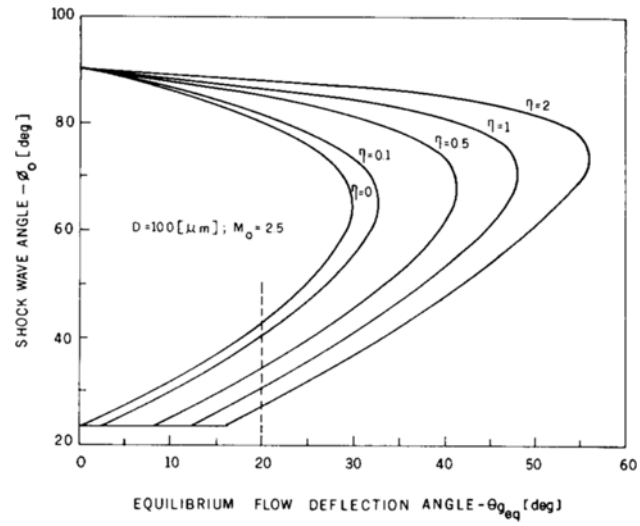

Fig. 11 The (ϕ, θ_g)-shock polar for $M_0=2.5$, $D=100\mu$m, $C=1000$J/(Kgm K), $\sigma=1000$Kgm/m^3, and different values of the loading ratio η.

becomes higher when η is increased. In addition, the maximum deflection angle, known as the detachment angle, is also seen to increase with increasing η. While for a dust-free (pure) gas (i.e., $\eta=0$) $(\theta_{g_{eq}})_{max}$ is about 29°, it reaches a value of about 56° when the loading ratio is $\eta=2$.

A typical (ϕ, θ_g)-polar is shown in Fig. 11 for the same conditions of Fig. 10. Here again $\theta_g=\theta_{g_{eq}}$. It is evident from this figure that if a certain deflection is required, say 20°, then as the loading ratio increases the angle of incidence, ϕ, which is needed to achieve the required deflection, decreases.

3. CONCLUSIONS

The flow field developed when a supersonic dusty gas suspension passes through a straight oblique shock wave has been investigated.

The investigation included a formulation of the governing equations of the flow field at hand and a numerical investigation of the dependence of the post shock suspension properties on the various physical properties of the solid particles.

ACKNOWLEDGEMENT

The financial support received from the U.S. Air Force under Grant AFOSR-86-0349 is acknowledged with thanks.

REFERENCES

Ben-Dor, G. and Igra, O., 1982, "The Relaxation Zone Behind Normal Shock Waves in a Dusty Reacting Gas, Part 1: Monatomic Gases", Journal of Plasma Physics, Vol. 27, pp. 377~395.

Carrier, G.F., 1958, "Shock Waves in a Dusty Gas", Journal Fluid Mechanics, Vol. 4, pp. 376~382.

Clift, R., Grace, J.R. and Weber, M.E. 1978, "Bubbles, Drops and Particles", Academic press, New York.

Drake, R.M., 1961, "Discussion on G.C. Vliet and G. Leppert Forced Convection Heat Transfer from an Isothermal Sphere to Water", ASME Journal Heat Transfer, Vol. 83, pp. 170~175.

Elata, D., Ben-Dor, G. and Igra, O., 1988, "The Effect of Particle Non-Uniformities of the Flow Field Behind Steady Normal Shock Waves", Submitted for publication.

Elperin, I., Ben-Dor, G. and Igra, O., 1986, "Analysis of Normal Shock Waves in a Carbon Laden Oxygen Gas", ASME Journal of Fluid Engineering, Vol. 108, pp. 354~359.

Gottlieb, J.J. and Coskunses, C.E., 1985, "Effects of Particle Volume on the Structure of a Partly Dispersed Normal Shock Wave in a Dusty Gas", UTIAS Report 295.

Igra, O. and Ben-Dor, G., 1980, "Parameters Affecting the Relaxation Zone Behind Normal Shock Waves in a Dusty Gas", Israel Journal of Technology, Vol. 18, pp. 159~168.

Igra, O. and Ben-Dor, G., 1984, "The Relaxation Zone Behind Normal Shock Waves in a Dusty Reacting Gas. Part 2: Diatomic Gases", Journal Plasma Physics, Vol. 31, pp. 115~140.

Kriebel, A.R., 1964, "Analysis of Normal Shock Waves in a Particle Laden Gas", Journal Basic Engineering, Transactions ASME, Ser, D86, pp. 655~663.

Marble, F.E., 1970, "Dynamics of Dusty Gases', Annual Review of Fluid Mechanics, vol. 2, pp. 397~466.

Mazor, G., Ben-Dor, G. and Igra, O., 1985, "A Simple and Accurate Expression for the Viscosity of Diatomic Gases up to 10000K", AIAA journal, Vol. 23, pp. 637~638.

Morgenthaler, J.H., 1962, "Analysis of Two-Phase Flow in Supersonic Exhausts", Progress in Astronautics and Aeronautics, Vol. 6, pp. 145~171.

Rudinger, G., 1973, "Wave Propagation in Suspension of Solid Particles in Gas Flow", Applied Mechanics Review, Vol. 26, pp. 273~279.

Rudinger, G., 1964, "Some Properties of Shock Relaxation in Gas Flow Carrying Small Particles", Physics of Fluids, Vol. 7, pp. 658~663.

Soo, S.L. 1967, "Fluid Dynamics of Multiphase Systems", 1967, Blaisdell Publishing Co., Waltham, Mass.

Van-Wylen, G.J. and Sonntag, R.E., 1978, "Fundamentals of Classical Thermodynamics", John Wiley & Sons, New York.